

Adaptive Anchor Policies for Efficient 4D Gaussian Streaming

Ashim Dahal¹, Rabab Abdelfattah¹, and Nick Rahimi¹

School of Computing Sciences and Computer Engineering, Hattiesburg, MS, USA
 {ashim.dahal,rabab.abdelfattah,nick.rahimi}@usm.edu

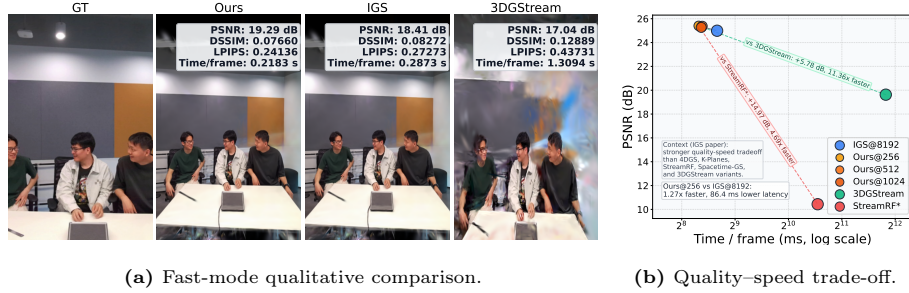


Fig. 1: Fast Rendering Mode. Our RL policy selects anchors that match or improve quality with $32\times$ fewer anchors on unseen data. Left: qualitative comparison (Ours, IGS, 3DGStream). Right: N3DV PSNR vs time/frame trade-off.

Abstract. Dynamic scene reconstruction with Gaussian Splatting has enabled efficient streaming for real-time rendering and free-viewpoint video. However, most pipelines rely on fixed anchor selection such as Farthest Point Sampling (FPS), typically using 8,192 anchors regardless of scene complexity, which over-allocates computation under strict budgets. We propose Efficient Gaussian Streaming (EGS), a plug-in, budget-aware anchor sampler that replaces FPS with a reinforcement-learned policy while keeping the Gaussian streaming reconstruction backbone unchanged. The policy jointly selects an anchor budget and a subset of informative anchors under discrete constraints, balancing reconstruction quality and runtime using spatial features of the Gaussian representation. We evaluate EGS in two settings: fast rendering, which prioritizes runtime efficiency, and high-quality refinement, which enables additional optimization. Experiments on dynamic multi-view datasets show consistent improvements in the quality-efficiency trade-off over FPS sampling. On unseen data, in fast rendering at 256 anchors ($32\times$ fewer than 8,192), EGS improves PSNR by $+0.52$ – 0.61 dB while running 1.29 – $1.35\times$ faster than IGS@8192 (N3DV and MeetingRoom). In high-quality refinement, EGS remains competitive with the full-anchor baseline at substantially lower anchor budgets. *Code and pretrained checkpoints will be released upon acceptance.*

Keywords: 4D Gaussian Splatting · 4D Gaussian Streaming · Reinforcement Learning

1 Introduction

Reconstructing dynamic scenes from multi-view observations is a fundamental problem in computer vision, enabling applications such as free-viewpoint video (FVV), novel-view synthesis (NVS), immersive media, and telepresence. Achieving high visual fidelity while maintaining real-time performance remains challenging, particularly when large numbers of scene primitives must be processed during rendering and reconstruction.

Neural radiance fields (NeRF) [29] have significantly advanced view synthesis by learning continuous volumetric representations of scenes. However, NeRF-based methods typically rely on computationally intensive volume rendering and per-scene optimization, which limits their efficiency for real-time applications. More recently, explicit scene representations have emerged as an efficient alternative. In particular, 3D Gaussian Splatting [13] represents scenes as collections of anisotropic Gaussians that can be efficiently rasterized, enabling high-quality rendering with substantially improved performance.

Building on Gaussian representations, recent works have explored streaming-based reconstruction pipelines that progressively select subsets of Gaussian anchors to balance reconstruction quality and computational efficiency. In these pipelines, anchor selection plays a critical role in determining both rendering fidelity and runtime cost. However, existing approaches commonly rely on heuristic strategies such as Farthest Point Sampling (FPS) [36], which allocate a fixed number of anchors regardless of scene complexity. While FPS promotes spatial coverage, it does not explicitly account for the varying importance of anchors across different scenes or viewpoints, potentially leading to inefficient allocation of computational resources.

This observation motivates adaptive and content-aware anchor selection for Gaussian streaming pipelines. Instead of relying on fixed heuristic sampling, anchor selection can be formulated as a decision-making problem that determines which anchors are most informative for reconstruction under a given computational budget. Based on this idea, we develop **Efficient Gaussian Streaming (EGS)**, a framework that learns to select informative anchors while maintaining compatibility with existing Gaussian streaming architectures.

Our contributions are summarized as follows:

- We analyze the limitations of fixed heuristic anchor selection in Gaussian streaming pipelines and show that it can lead to inefficient allocation of computation under strict budgets.
- We introduce **Efficient Gaussian Streaming (EGS)**, a plug-in, budget-aware sampler that adaptively selects both an anchor budget and a subset of informative anchors while keeping the streaming backbone unchanged.
- We develop a two-stage learning scheme (SFT warm-start followed by RL Contextual Bandit optimization) with a reward that explicitly trades off sparsity, runtime, and reconstruction quality.
- Extensive experiments on N3DV and MeetingRoom demonstrate consistent improvements in the quality–efficiency trade-off over FPS-based sampling.

2 Related Work

Novel view synthesis and efficient scene representations. Novel view synthesis has been widely studied with implicit neural representations such as NeRF and dynamic variants that model time via deformation or conditioning [26, 29, 32, 33, 35], supported by multi-view video benchmarks for free-viewpoint video [6, 23, 34, 38]. Complementary approaches improve efficiency via factorized space–time fields [2, 8] and explicit point-based representations; in particular, 3D Gaussian Splatting (3DGS) enables real-time rendering with differentiable rasterization and has become a strong foundation for interactive view synthesis [13], with ongoing work improving efficiency and scalability [10, 42, 55].

Dynamic Gaussian splatting. Dynamic extensions of splatting model motion and time-varying appearance using explicit Gaussian primitives [7, 25, 49, 52]. Recent work explores broader capture settings and additional priors, including multi-view consistency, physics, or hybrid representations [3, 5, 12, 14, 15, 24, 28, 31, 39, 46, 54, 57]. These methods can achieve strong quality, but many remain offline or do not explicitly target strict streaming budgets.

Streaming and online dynamic reconstruction. Streaming radiance fields have been studied via incremental learning and residual representations [22, 44]. Gaussian streaming methods pursue low-latency updates either by training Gaussians on-the-fly [40] or by using generalizable feed-forward motion prediction driven by a compact set of anchors [20, 37, 51]. IGS is particularly relevant as it standardizes an anchor-driven streaming pipeline and motivates plug-in improvements to anchor selection under fixed budgets [51].

Anchor selection under budget constraints. Anchor-driven streaming critically depends on selecting a subset of Gaussians under strict compute and point budgets. Existing systems typically use hand-crafted heuristics—most notably farthest point sampling (FPS)—to promote spatial coverage [36, 51]. While learned selection under resource constraints has been explored elsewhere [4, 11, 16, 45, 50], applying it to anchor-based Gaussian streaming with *joint budget+subset* constraints remains underexplored. Our work targets *budgeted* anchor selection by learning a context-aware policy that directly optimizes the quality–runtime trade-off within the IGS streaming interface [51].

Learning policies for resource allocation. Reinforcement learning and contextual bandits provide principled tools for allocating limited computation based on observed context [17, 21, 41]. Policy-gradient methods offer a general mechanism for optimizing stochastic selection policies [48]. Attention-based set encoders further provide a natural architecture for scoring and selecting elements from unordered candidate sets [18, 43]. EGS combines these perspectives to learn budgeted anchor selection for streaming 4DGS under strict fast-mode evaluation with same-budget comparisons.

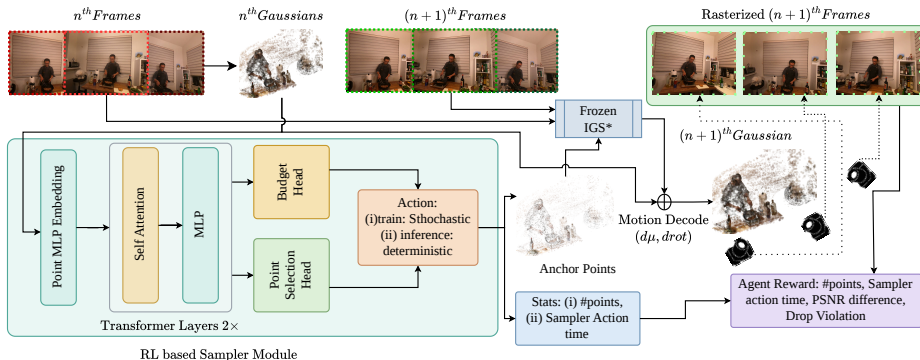


Fig. 2: Method overview of EGS. Our adaptive sampler selects a budgeted set of anchor Gaussians (stochastic during training; deterministic at inference) using point-MLP embeddings and a lightweight Transformer [18,43], then feeds the selected anchors to the frozen IGS pipeline for anchor-graph construction and rasterization [51]. The training objective trades off sparsity, runtime, and PSNR against FPS-based teacher targets [9,36].

3 Methodology

We introduce Efficient Gaussian Streaming (EGS) as a learned plug-in sampler that selects anchors under an explicit budget while keeping the downstream IGS reconstruction and rasterization stack frozen [51]. Fig. 2 summarizes the pipeline and the training/inference behavior.

3.1 Problem Setup: Budgeted Anchor Selection

For frame t , let the (masked) set of available Gaussians be $\mathcal{G}_t = \{(\mathbf{x}_j, o_j, \mathbf{s}_j)\}_{j=1}^{N_t}$, where $\mathbf{x}_j \in \mathbb{R}^3$ denotes the center, o_j opacity, and $\mathbf{s}_j \in \mathbb{R}^3$ the scale. We filter to a scene bounding box and cap the pool via voxel-hash downsampling [30], yielding a bounded candidate set $\mathcal{C}_t = \{c_m\}_{m=1}^{M_t}$ with $M_t \leq M_{\max}$ (we use $M_{\max} = 16384$). The sampler outputs the action

$$a_t = (\kappa_t, \Omega_t), \quad \kappa_t \in \mathcal{B}, \quad \Omega_t \subseteq \{1, \dots, M_t\}, \quad |\Omega_t| = \kappa_t, \quad (1)$$

where κ_t is the selected anchor budget and Ω_t the selected subset of indices. In all experiments, \mathcal{B} is a fixed set of discrete budgets (256–8192). The selected anchors are passed to the *unchanged* IGS anchor-graph construction (neighbors and interpolation weights) and the frozen renderer.

3.2 Sampler Policy

Each candidate $c_m \in \mathcal{C}_t$ is represented by a compact descriptor

$$\xi_m = [\tilde{\mathbf{x}}_m, o_m, \log(\bar{s}_m + \epsilon), d_m] \in \mathbb{R}^6, \quad (2)$$

where $\tilde{\mathbf{x}}_m$ are bounding-box normalized coordinates, \bar{s}_m is mean scale, and d_m is the normalized distance to the candidate-cloud center. A point-wise MLP followed by a small Transformer encoder maps $\{\xi_m\}$ to token embeddings, from which the policy predicts (i) a categorical distribution over budgets and (ii) per-candidate selection probabilities. Self-attention lets the policy score each candidate in the context of the full candidate set, modeling interactions among Gaussians within the current scene state. We omit architectural minutiae for brevity; the full configuration is provided in Sec. 4.

3.3 Training Objective

Training follows a two-stage protocol: (i) *Imitation warm-start*. We initialize the sampler by imitating FPS anchors. Because the policy operates on a capped candidate pool, supervision is overlap-based: candidates that coincide with teacher anchors are labeled positive. The warm-start optimizes a selection loss (BCE-with-logits) plus a budget classification loss (cross-entropy). (ii) *Contextual-bandit optimization*. We then optimize the sampler with a policy-gradient objective in a frame-wise contextual bandit [21]. Let $\psi(\hat{I}, I)$ denote PSNR between a rendered image \hat{I} and ground truth I . We define a teacher target by mixing two FPS references: an 8k reference (used for time normalization and compatibility with IGS) and a stronger 16k teacher (used in training only for stability/upper bound).

$$\psi_{\text{tgt}} = \eta \psi_{\text{ref}} + (1 - \eta) \psi_{\text{tea}}. \quad (3)$$

The reward trades off sparsity, runtime, and quality:

$$\begin{aligned} \rho_t = & -\lambda_\kappa \frac{\kappa_t}{\kappa_{\max}} - \lambda_t \max\left(0, \frac{t_{\text{RL}}}{t_{\text{ref}}} - 1\right) - \lambda_v \max(0, \psi_{\text{tgt}} - \psi_{\text{RL}} - \delta) \\ & + \lambda_g \max(0, \psi_{\text{RL}} - \psi_{\text{tgt}}), \end{aligned} \quad (4)$$

where t_{RL} is sampler+render time, t_{ref} is the FPS@8k time, δ is a PSNR tolerance, and $\kappa_{\max} = 8192$. Scalar weights $\{\lambda_\kappa, \lambda_t, \lambda_v, \lambda_g\}$ are used for budget, time, violation, and gain terms; δ is a PSNR tolerance. We use an exponential-moving-average baseline $\bar{\rho} \leftarrow \mu \bar{\rho} + (1 - \mu) \rho_t$ and optimize a REINFORCE style surrogate:

$$\mathcal{L}_{\text{pg}} = -(\rho_t - \bar{\rho}) \log \pi_\theta(a_t | \mathcal{C}_t) - \beta \mathcal{H}(\pi_\theta(\cdot | \mathcal{C}_t)), \quad (5)$$

where $\log \pi_\theta(a_t | \mathcal{C}_t)$ sums budget and subset log-probabilities and $\mathcal{H}(\cdot)$ denotes entropy [41, 48]. We found the training regime to be insensitive to moderate weight changes as anchor budget stabilizes after a few thousand training steps Fig. 3a.

3.4 Deterministic Inference

At inference, we use a deterministic deployment rule: the budget κ_t can be fixed by the user to meet a target compute/latency constraint, or predicted by the policy via argmax; anchors are then selected by top- κ_t scores. The resulting Ω_t is fed to the frozen IGS anchor-graph construction and renderer to produce the final frame.

4 Experiments

4.1 Datasets and Splits

We train our model using the N3DV dataset [23], with 11,762 training pairs and 118 validation pairs from the scenes {Coffee Martini, Cook Spinach, Flame Salmon, Flame Steak}. We evaluate the performance of our model and competing methods on N3DV using the 118 validation pairs and additionally on unseen scenes {Sear Steak, Cut Roasted Beef}. To assess dataset-shift generalization, we further evaluate our model and competing methods on the MeetingRoom dataset [22], using the scenes {Discussion, Trimming}. The {Vrheadset} scene is excluded due to severe distortion.

4.2 Training Setup

The candidate pool was capped at $M_{\max} = 16384$ via voxel-hash downsampling within a scene bounding box. Budgets were selected from fixed discrete buckets spanning 256–8192 anchors. The sampler used a point-wise MLP followed by a 2-layer Transformer encoder ($d=128$, 4 heads, dropout 0.1). Optimization used AdamW [27] (lr 1×10^{-4} , weight decay 0.01, betas 0.9/0.95) with gradient clipping at 1.0. Training followed 1 epoch imitation warm-start, then policy-gradient updates with an EMA reward baseline and entropy regularization. Random seeds were fixed (2026) across Python/NumPy/PyTorch. The preserved multi-scene runs accounted for ≈ 23.4 single NVIDIA A100 GPU hours; the main run checkpoint corresponded to 7,350 completed policy-gradient steps.

4.3 Evaluation Protocol

Because prior Gaussian streaming systems make different interface and runtime assumptions, we use IGS as the primary reference and report 3DGStream/StreamRF for contextual comparison only [22, 40]. We evaluate under two fixed protocols:

Fast Rendering Mode (primary). We disable online refinement and run feed-forward inference with a frozen sampler checkpoint and frozen IGS backbone (per-frame reconstruction and rendering).

High-Quality (HQ) Refinement Mode (context). We enable local refinement to prioritize visual quality. External methods do not share an identical plug-in sampling interface and typically do not expose sampler latency; HQ results are therefore reported as protocol-level context rather than strict latency comparisons.

Main Evaluation Lens. Fast rendering is the main evaluation lens in this paper; high-quality refinement is included for quality-oriented completeness. We additionally provide a hybrid deployment option in the supplemental code, while reporting results under the two protocols separately. For evaluation, we report standard image quality and efficiency metrics including PSNR (\uparrow), DSSIM (\downarrow), LPIPS (\downarrow), rendering time per frame (\downarrow), render FPS (\uparrow), and sampler latency (\downarrow) [47, 56].

Table 1: N3DV (Fast Rendering Mode), per-scene results (unseen scenes). The scenes in this table are **not previously seen by the RL sampler** during training, and therefore measure generalization to unseen content. Metrics: **PSNR** \uparrow , **DSSIM/LPIPS** \downarrow , **Time/frame** (s) \downarrow , **Render FPS** \uparrow , and **Sampler latency** (ms) \downarrow . “–” indicates unavailable metrics. **Best** and **second-best** indicate the top-1 and top-2 values (per column), respectively. *StreamRF* rows are shown in gray for context.

Scene	Method	Budget	PSNR \uparrow	DSSIM \downarrow	LPIPS \downarrow	T/f \downarrow	FPS \uparrow	Samp. \downarrow
	StreamRF [22]	–	13.478	0.252	0.883	0.029	34.29	–
	3DGStream [40]	–	19.195	0.145	0.551	1.741	0.57	–
Sear	IGS [51]	8192	26.588	0.045	0.130	0.356	160.91	30.52
Steak	Ours (tiny)	256	27.609	0.043	0.111	0.271	160.25	31.91
	Ours (small)	512	27.299	0.045	0.113	0.278	154.82	32.23
	Ours (med.)	1024	27.654	0.041	0.105	0.286	118.85	33.07
	StreamRF [22]	–	12.158	0.280	0.883	0.029	34.02	–
	3DGStream [40]	–	19.102	0.137	0.387	1.434	0.70	–
Cut	IGS [51]	8192	22.203	0.080	0.219	0.319	158.59	32.65
Roasted	Ours (tiny)	256	22.392	0.074	0.199	0.229	157.39	30.65
Beef	Ours (small)	512	22.284	0.078	0.208	0.232	141.62	30.92
	Ours (med.)	1024	22.085	0.079	0.215	0.236	161.13	31.50

4.4 Evaluation on N3DV Dataset

We evaluate the proposed EGS framework on the N3DV dataset, following the standard protocol used by prior work reference [1, 5, 19, 22, 31, 40, 51, 53]. The RL sampler is trained on a predefined split over four N3DV training scenes, with a held-out validation partition from the same scenes discussed in Sec. 4.1. To analyze the effect of anchor allocation on reconstruction quality and efficiency, we evaluate our method using three anchor configurations: **tiny** (256 anchors), **small** (512 anchors), and **medium** (1024 anchors). These configurations are compared against the IGS baseline, which uses a fixed budget of 8192 anchors. The other baselines are anchor free; thus not directly comparable.

Generalization to unseen scenes. We first evaluate the model on two scenes that are completely unseen during sampler training. The results are reported in Tab. 1. Across these scenes, EGS consistently improves reconstruction quality while reducing rendering cost. Averaged over the two scenes, EGS (tiny) improves PSNR by **+0.605 dB** compared to IGS while reducing DSSIM and LPIPS by **0.004** and **0.019**, respectively. At the same time, the rendering time per frame decreases from **0.337 s** to **0.250 s**, corresponding to a **1.349 \times speedup**. These results indicate that the learned sampler generalizes effectively to scenes that were not observed during training.

Held-out validation scenes. We next evaluate the method on the 20% held-out split of the four training scenes, with results summarized in Tab. 2. When averaged across the seen scenes, EGS (tiny) improves PSNR by **+0.462 dB** relative to IGS while reducing DSSIM and LPIPS by **0.003** and **0.008**, respectively. In addition, the rendering time per frame decreases from **0.437 s** to **0.356 s**, resulting in a **1.229 \times speedup**. Overall, the results across both seen and unseen

Table 2: N3DV (Fast Rendering Mode), per-scene results (validation held-out). Results are reported on the remaining held-out split for evaluation highlighted in Sec. 4.1. Metrics: **PSNR** \uparrow , **DSSIM/LPIPS** \downarrow , **Time/frame** (s) \downarrow , **Render FPS** \uparrow , and **Sampler** latency (ms) \downarrow . “–” indicates unavailable metrics. **Best** and **second-best** indicate the top-1 and top-2 values (per column), respectively. *StreamRF* rows are shown in gray for context.

Scene	Method	Budget	PSNR \uparrow	DSSIM \downarrow	LPIPS \downarrow	T/f \downarrow	FPS \uparrow	Samp. \downarrow
	StreamRF [22]	–	12.433	0.224	0.877	0.029	34.00	–
	3DGStream [40]	–	17.926	0.146	0.506	4.844	0.21	–
Coffee	IGS [51]	8192	25.887	0.044	0.111	0.448	108.44	38.12
Martini	Ours (tiny)	256	26.021	0.043	0.110	0.338	132.41	33.74
	Ours (small)	512	26.283	0.041	0.108	0.339	132.61	33.58
	Ours (med.)	1024	26.178	0.042	0.107	0.357	133.09	34.33
	StreamRF [22]	–	12.186	0.212	0.885	0.033	29.97	–
	3DGStream [40]	–	22.273	0.080	0.341	4.441	0.23	–
Cook	IGS [51]	8192	23.937	0.051	0.166	0.424	164.44	33.82
Spinach	Ours (tiny)	256	24.085	0.049	0.158	0.364	162.97	40.89
	Ours (small)	512	24.037	0.049	0.160	0.393	161.48	34.24
	Ours (med.)	1024	24.008	0.051	0.160	0.357	158.95	34.73
	StreamRF [22]	–	12.495	0.225	0.900	0.029	34.61	–
	3DGStream [40]	–	19.634	0.125	0.444	5.663	0.18	–
Flame	IGS [51]	8192	26.343	0.039	0.099	0.480	133.94	37.61
Salmon	Ours (tiny)	256	26.911	0.036	0.094	0.393	138.40	34.52
	Ours (small)	512	26.985	0.035	0.093	0.432	128.31	34.50
	Ours (med.)	1024	26.436	0.038	0.096	0.413	121.70	41.44
	StreamRF [22]	–	13.155	0.191	0.867	0.031	32.32	–
	3DGStream [40]	–	16.767	0.122	0.589	3.840	0.26	–
Flame	IGS [51]	8192	26.244	0.046	0.151	0.398	160.71	29.76
Steak	Ours (tiny)	256	27.240	0.038	0.134	0.329	155.58	36.23
	Ours (small)	512	27.138	0.040	0.139	0.345	156.94	38.74
	Ours (med.)	1024	26.903	0.042	0.144	0.336	157.24	35.38

scenes demonstrate that the proposed RL-based sampler can significantly reduce the number of anchors while maintaining or improving reconstruction quality.

4.5 Results on MeetingRoom

We further evaluate the proposed method on the MeetingRoom dataset, with results reported in Tab. 3. Compared to the IGS baseline using 8192 anchors, EGS operates with significantly smaller anchor budgets (256–1024 anchors), corresponding to up to a **32 \times reduction in anchor count**. Despite this large reduction, the proposed sampler maintains or improves reconstruction quality while simultaneously improving rendering efficiency. Averaged across both scenes, EGS (tiny) improves PSNR by **+0.519 dB** relative to IGS@8192 and reduces DSSIM/LPIPS by **0.005/0.030**. At the same time, the average rendering time per frame decreases from **0.285 s** to **0.222 s**, corresponding to a **1.29 \times speedup**. These results indicate that the learned policy can effectively select informative anchors while maintaining strict budget constraints. When compared to the next available streaming baseline (3DGStream), the proposed

Table 3: MeetingRoom (Fast Rendering Mode), per-scene results. The scenes in this table are evaluated under the same protocol. Metrics: **PSNR** \uparrow , **DSSIM/LPIPS** \downarrow , **Time/frame** (s) \downarrow , **Render FPS** \uparrow , and **Sampler latency** (ms) \downarrow . “–” indicates unavailable metrics. **Best** and **second-best** indicate the top-1 and top-2 values (per column), respectively. *StreamRF* rows are shown in gray for context.

Scene	Method	Budget	PSNR \uparrow	DSSIM \downarrow	LPIPS \downarrow	T/f \downarrow	FPS \uparrow	Samp. \downarrow
Discussion	StreamRF [22]	–	12.845	0.199	0.877	0.063	15.99	–
	3DGStream [40]	–	17.040	0.129	0.437	1.309	0.76	–
	IGS [51]	8192	18.409	0.083	0.273	0.287	197.02	25.98
	Ours (tiny)	256	18.992	0.077	0.244	0.211	192.70	30.62
	Ours (small)	512	18.502	0.078	0.249	0.213	197.71	30.93
	Ours (med.)	1024	19.289	0.077	0.241	0.218	186.09	31.65
Trimming	StreamRF [22]	–	13.415	0.200	0.884	0.057	17.60	–
	3DGStream [40]	–	16.447	0.169	0.449	1.211	0.83	–
	IGS [51]	8192	17.939	0.080	0.303	0.283	136.76	23.65
	Ours (tiny)	256	18.394	0.077	0.272	0.232	186.60	32.80
	Ours (small)	512	18.358	0.077	0.284	0.217	198.34	30.55
	Ours (med.)	1024	17.836	0.079	0.293	0.217	190.85	31.48

method achieves substantially better efficiency while also improving reconstruction quality. In particular, EGS improves PSNR by $+1.949$ dB on average while reducing the rendering time per frame from **1.260 s** to **0.222 s**, yielding a **5.68 \times speedup**. These gains demonstrate that adaptive anchor selection allows the system to allocate computational resources more effectively than fixed-budget streaming approaches. Finally, the consistent improvements observed across both MeetingRoom scenes suggest that the learned sampler does not rely on scene-specific memorization. Instead, it learns a generalizable strategy for selecting informative anchors that transfers well across datasets with different geometry, motion patterns, and visual characteristics.

4.6 Training and RL Analysis

To better understand the behavior of the proposed RL-based sampler, we analyze its training dynamics, convergence properties, and generalization behavior. **Budget stabilization.** As shown in Fig. 3a, anchor selection rapidly transitions from an exploratory phase into a stable regime close to the desired budget. During the early training steps the sampler explores a wide range of anchor counts, but the policy quickly learns to enforce the budget constraint. Different training runs exhibit distinct exploration behaviors—for example, the v2 run explores more aggressively and shows larger variance compared to v1—but both eventually converge to the same budget-controlled operating point. This consistent behavior across runs indicates that the sampler learns a robust budget-enforcement policy rather than overfitting to a particular initialization or reward-weight configuration. **Convergence.** The reward signal and its EMA baseline stabilize smoothly during training, as illustrated in Fig. 3b, indicating stable contextual-bandit updates. In parallel, the on-policy Δ PSNR signal shown in Fig. 3c initially improves as exploration discovers better anchor-selection strategies and

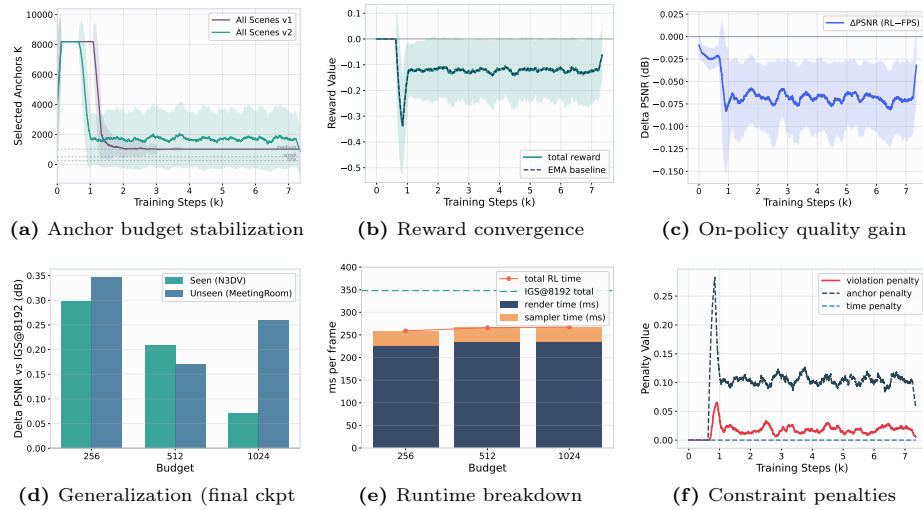


Fig. 3: Training dynamics and analysis. Across training, the sampler learns stable budget control and converges under constraint-aware rewards; final checkpoints show positive Δ PSNR vs IGS@8192 on seen and unseen splits. Training curves use stochastic actions and may differ from deterministic inference.

then gradually plateaus as exploration decays. The timing of this plateau aligns with the budget stabilization observed in panel, suggesting that once the policy identifies reliable anchor-selection patterns it transitions from broad exploration to consistent exploitation. **Generalization and efficiency.** Panels (d-f) further analyze the performance of the trained policy. The generalization results in Fig. 3d show that PSNR improvements over IGS@8192 remain positive across both seen scenes (N3DV) and unseen scenes (MeetingRoom), indicating that the sampler learns transferable anchor-selection strategies rather than memorizing scene-specific patterns. Runtime decomposition in Fig. 3e shows that the sampling overhead remains small compared to rendering time, confirming that the learned policy does not introduce significant computational cost. Finally, Fig. 3f (f) shows that constraint penalties remain bounded after the initial exploration phase, indicating that the learned policy respects both the anchor-budget and runtime constraints while maintaining improved reconstruction quality.

4.7 Qualitative Results

We present qualitative comparisons to illustrate the visual fidelity and temporal consistency of the proposed method. Fig. 4 compares representative frames from eight scenes, with zoomed-in regions emphasizing thin structures, high-frequency textures, and motion boundaries. The crop locations are fixed per scene and applied to all methods to highlight regions where artifacts are most visible. Overall, our method better preserves local detail and reduces temporal artifacts (flicker/ghosting) compared to the streaming baselines. Temporal progression is illustrated in Fig. 5, which shows our reconstruction over time in the *Trimming*

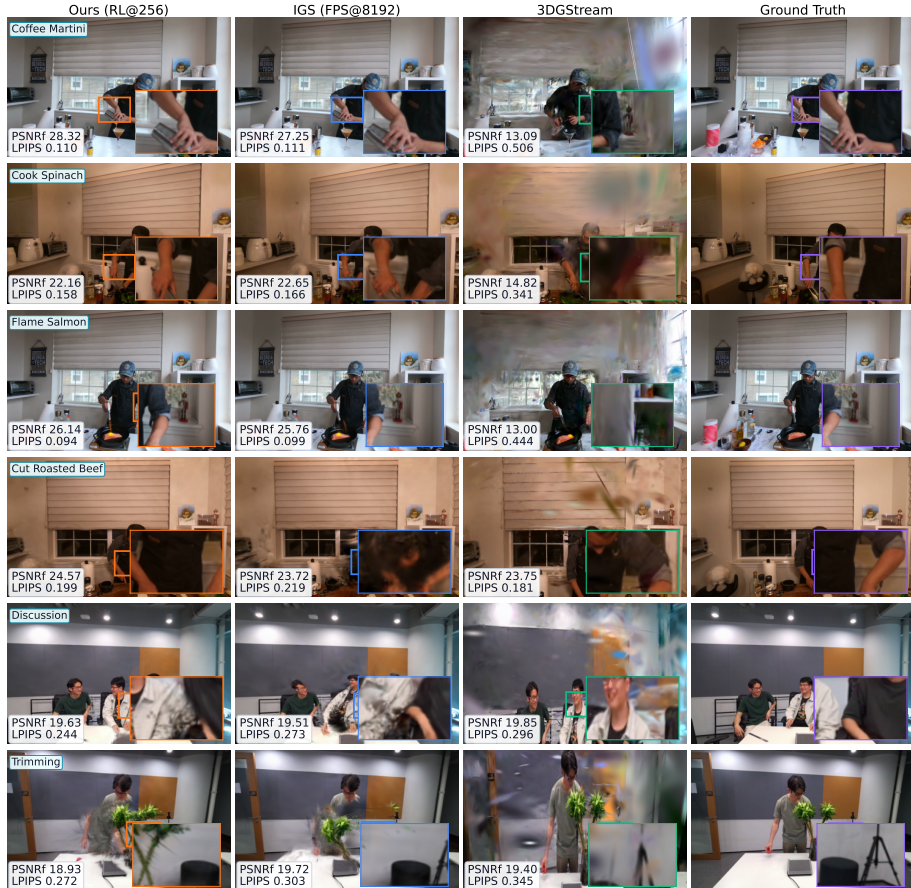


Fig. 4: Qualitative comparison on N3DV and MeetingRoom scenes. We compare our method against IGS, 3DGStream, and ground truth across representative scenes.

scene of MeetingRoom. We observe coherent edges and fewer drifting artifacts across timesteps, supporting the temporal consistency of the learned sampling strategy.

4.8 Ablation Study

We conduct ablation studies to analyze the effect of anchor budgets, training strategies, and subset selection on reconstruction quality and efficiency.

Budget frontier (fast mode). Table 4 sweeps the anchor sampling budget and analyzes the quality–speed trade-off on N3DV. The strongest Pareto region appears in the low-budget range (256–1024). In this regime, our sampler consistently improves PSNR compared to both the FPS-matched baseline and the IGS@8192 reference. For example, the gain over IGS reaches $\Delta P_{IGS} = +0.6498$

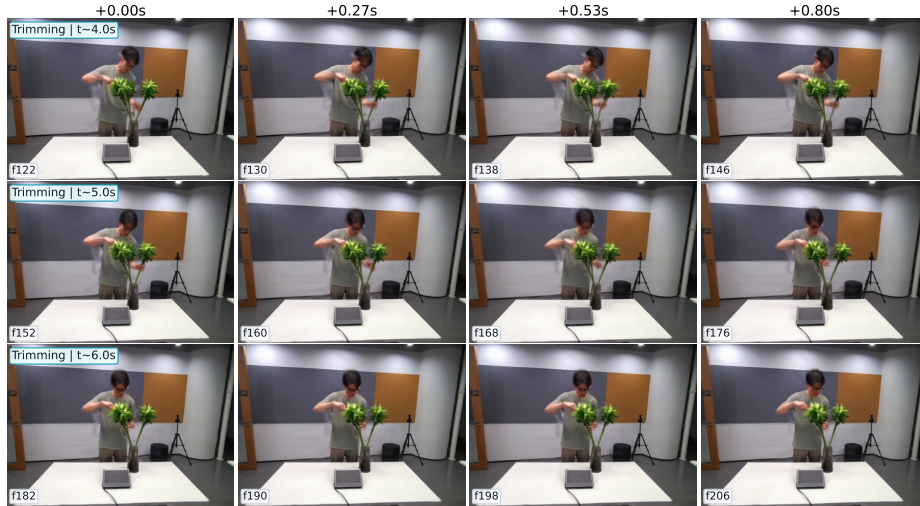


Fig. 5: Motion progression on MeetingRoom:Trimming. Reconstructions across frames demonstrating temporal consistency.

Table 4: N3DV fast-mode budget frontier. Budget sweep on N3DV. ΔP_{FPS} denotes PSNR gain over the FPS baseline and ΔP_{IGS} denotes gain over IGS@8192. **RT** is the runtime ratio defined as $\text{time}(\text{baseline})/\text{time}(\text{ours})$, where values > 1 indicate that our method is faster. Best/second-best computed within 256–1024.

Budget	ΔP_{FPS} (PSNR) \uparrow	ΔP_{IGS} (PSNR) \uparrow	RT vs FPS (\uparrow faster)	RT vs IGS (\uparrow faster)
256	0.4244	0.6498	0.8532 \times	1.2506\times
512	0.4792	0.5883	0.8428\times	1.1944 \times
1024	0.4576	0.5372	0.8860\times	1.2092\times
2048	0.2564	0.2887	0.8875 \times	1.1741 \times
3072	-0.2720	-0.2349	0.9115 \times	1.1581 \times
4096	-0.3392	-0.3163	0.9232 \times	1.1105 \times
6144	-0.0965	-0.0883	0.9321 \times	1.0292 \times
8192	0.3486	0.3486	0.9436 \times	0.9436 \times

at budget 256 and +0.5372 at 1024. At the same time, the method remains faster than IGS, achieving runtime speedups of 1.2506 \times and 1.2092 \times at budgets 256 and 1024, respectively. As the sampling budget increases beyond this range, the marginal improvement diminishes and the frontier gradually flattens.

Training variants (SFT vs. RL vs. SFT+RL). We compare three training strategies: supervised fine-tuning (SFT), reinforcement learning (RL), and their combination (SFT+RL). Tab. 5 reports training-time evaluation using policy-trainer proxy metrics on a two-scene run. The SFT-only variant collapses to the full sampling budget throughout training (tail budget 8192), indicating that supervised pretraining alone does not enforce the compute constraint. The RL-only variant learns to operate at lower budgets but exhibits higher variance and remains close to runtime parity with the FPS baseline. In contrast, the combined SFT+RL strategy achieves the most stable steady-state behavior, concentrating in the low–mid budget regime while improving speed (tail speed 1.169 \times),

Table 5: SFT vs. RL vs. SFT+RL (training evaluation). Two-scene run (Coffee Martini + Cook Spinach), 1k steps. We report tail-60-step averages from the policy trainer logs. Speed is FPS/RL (> 1 faster).

Variant	Tail budget ↓	PSNR drop ↓	Speed ↑	Reward ↑
SFT-only	8192.0	0.0167	0.999×	0.0000
RL-only	1625.6	0.0591	0.981×	-0.1287
SFT+RL	1433.6	0.0622	1.169×	-0.1161

Table 6: Low-budget vs IGS@8192. Fast- and HQ-mode averages. Δ PSNR is relative to IGS@8192 (per mode); speed is time(IGS)/time(method) (> 1 faster). **Fast scope:** N3DV + MeetingRoom. **HQ scope:** N3DV (Sear Steak, Cut Roasted Beef) + MeetingRoom (Discussion, Trimming). **Best** and **second-best**: top-1/top-2.

Mode	Method	PSNR ↑	Δ PSNR vs IGS ↑	Speed vs IGS ↑
fast	IGS (8192)	23.444	0.000	1.00×
fast	Ours (tiny)	23.955	0.512	1.27×
fast	Ours (small)	23.861	0.417	1.22×
fast	Ours (med.)	23.799	0.355	1.24×
quality	IGS (8192)	30.742	0.000	1.00×
quality	Ours (tiny)	30.748	0.006	1.05×
quality	Ours (small)	30.821	0.080	1.03×
quality	Ours (med.)	30.442	-0.300	1.07×

suggesting that SFT provides a stable initialization for subsequent bandit-based learning.

Low-budget variants vs. IGS@8192. Tab. 6 compares low-budget configurations against the IGS@8192 reference under two evaluation protocols: **fast** mode (prioritizing throughput) and **HQ** mode (prioritizing reconstruction fidelity). In **fast** mode, Ours (tiny) achieves the best quality–speed trade-off, improving PSNR by +0.512 while running 1.27× faster than IGS@8192. Under **HQ** mode, the ranking changes: Ours (small) delivers the largest quality improvement (+0.080), whereas Ours (med.) achieves the greatest speedup (1.07×).

Same-budget subset selection (fast mode). To disentangle gains from *budget* versus *subset choice*, we compare our RL sampler to an FPS-matched baseline at the *same* anchor budget. As summarized in Tab. 7, RL improves PSNR in **14/15** scene–budget pairs in fast mode, with consistent average gains of +**0.424**, +**0.479**, and +**0.458** dB at budgets 256/512/1024, respectively. This shows the improvements are not solely due to operating at lower budgets, but arise from selecting a higher-quality subset under the same compute envelope (with FPS/RL ratios of 0.853×–0.886×).

HQ averages across datasets. Tab. 8 summarizes HQ performance on MeetingRoom and N3DV. While IGS@8192 remains the strongest baseline in MeetingRoom HQ, our low-budget variants remain competitive (e.g., 28.943 PSNR at 512 vs 29.553 for IGS) and preserve favorable runtime trends (lowest T/f at 1024). On N3DV HQ, low-budget sampling improves quality beyond IGS@8192

Table 7: Same-budget ablation (Fast mode): RL vs FPS-matched baseline. At equal budgets, the RL sampler improves PSNR over an FPS-matched baseline in 14/15 scene-budget pairs. We report win counts and average Δ PSNR (RL–FPS) with the runtime ratio FPS/RL (values < 1 indicate RL is slower than the FPS baseline).

Budget	Wins	Δ PSNR \uparrow	FPS/RL
256	4/5	+0.424	0.853 \times
512	5/5	+0.479	0.843 \times
1024	5/5	+0.458	0.886 \times

Table 8: HQ refinement (dataset averages). Averages over MeetingRoom (Discussion, Trimming) and N3DV (Sear Steak, Cut Roasted Beef; HQ). External baselines for MeetingRoom and Cut Roasted Beef use full local HQ runs; sampler latency is unavailable for external methods. **Best** and **second-best**: top-1/top-2 per column.

Dataset	Method	Budget	PSNR \uparrow	DSSIM \downarrow	LPIPS \downarrow	T/f (s) \downarrow	FPS \uparrow
MeetingRoom	StreamRF [22]	8192	12.132	0.235	0.880	2.713	0.41
	3DGStream [40]	8192	19.808	0.103	0.321	4.491	0.22
	IGS [51]	8192	29.553	0.031	0.128	0.668	198.49
	Ours (tiny)	256	28.760	0.035	0.136	0.656	166.41
	Ours (small)	512	28.943	0.034	0.134	0.689	166.56
	Ours (med.)	1024	28.879	0.034	0.135	0.621	139.44
N3DV	StreamRF [22]	8192	21.263	0.294	0.852	8.248	4.49
	3DGStream [40]	8192	28.557	0.102	0.367	10.526	102.12
	IGS [51]	8192	31.930	0.022	0.092	1.006	161.60
	Ours (tiny)	256	32.736	0.021	0.084	0.943	160.21
	Ours (small)	512	32.700	0.021	0.084	0.940	137.47
	Ours (med.)	1024	32.006	0.022	0.091	0.949	120.65

(best PSNR 32.736 at 256), confirming that the learned sampling can translate to refinement settings when HQ records are available.

Training robustness (analysis). Across runs with different reward weights, the policy returns to the intended budget regime and maintains bounded constraint penalties (Fig. 3), supporting that the observed Pareto improvements are not due to unstable or unconstrained behavior.

5 Conclusion

We presented Efficient Gaussian Streaming: a budget-aware RL sampling method for streaming 4D Gaussian Splatting, designed to select anchors under strict per-frame constraints. Under the primary fast-rendering protocol, the method improves the budget frontier on N3DV and MeetingRoom datasets, with consistent low-budget gains and modest overhead. Same-budget comparisons suggest that improvements arise from better subset selection rather than budget changes. Future works would expand protocol-aligned evaluation and explore tighter sampler–refiner coupling for stronger quality under fixed streaming budgets.

Limitations

Our method is evaluated primarily in Fast Rendering Mode with frozen components, and extending the policy to HQ refinement or jointly optimizing refinement and sampling remains future work. The policy introduces modest inference overhead, so our advantages are most pronounced in low-budget regimes where better selection offsets this cost.

The approach is tailored to the IGS candidate-pool and graph interface, and transferring it to substantially different backbones may require adapting the descriptor and masking. Finally, the RL objective relies on a hand-designed reward and teacher signal; while effective, alternative objectives and more explicit temporal modeling may further improve robustness under extreme dynamics.

Acknowledgements

TBA in Final Paper

References

1. Bae, J., Kim, S., Yun, Y., Lee, H., Bang, G., Uh, Y.: Per-gaussian embedding-based deformation for deformable 3d gaussian splatting. In: European Conference on Computer Vision. pp. 321–335. Springer (2024) 7
2. Cao, A., Johnson, J.: Hexplane: A fast representation for dynamic scenes. 2023 IEEE/CVF Conference on Computer Vision and Pattern Recognition (CVPR) pp. 130–141 (2023), <https://api.semanticscholar.org/CorpusID:256105095> 3
3. Deng, J., Shi, P., Li, Q., Guo, J.: Dynasplat: Dynamic-static gaussian splatting with hierarchical motion decomposition for scene reconstruction. arXiv preprint arXiv:2506.09836 (2025) 3
4. Dovrat, O., Lang, I., Avidan, S.: Learning to sample. In: CVPR (2019), https://www.eng.tau.ac.il/~avidan/papers/Dovrat_Learning_to_Sample_CVPR_2019_paper.pdf 3
5. Duan, Y., Wei, F., Dai, Q., He, Y., Chen, W., Chen, B.: 4d-rotor gaussian splatting: towards efficient novel view synthesis for dynamic scenes. In: ACM SIGGRAPH 2024 Conference Papers. pp. 1–11 (2024) 3, 7
6. Fang, Q., Shuai, Q., Dong, J., Bao, H., Zhou, X.: Reconstructing 3d human pose by watching humans in the mirror. In: CVPR (2021) 3
7. Feng, C., Tang, Z., Yu, W., Pang, Y., Zhao, Y., Zhao, J., Yuan, L., Tian, Y.: E-4dgs: High-fidelity dynamic reconstruction from the multi-view event cameras. arXiv preprint arXiv:2508.09912 (2025) 3
8. Fridovich-Keil, S., Meanti, G., Warburg, F.R., Recht, B., Kanazawa, A.: K-planes: Explicit radiance fields in space, time, and appearance. In: Proceedings of the IEEE/CVF Conference on Computer Vision and Pattern Recognition (CVPR). pp. 12479–12488 (June 2023) 3
9. Gonzalez, T.F.: Clustering to minimize the maximum intercluster distance. Theoretical Computer Science **38**, 293–306 (1985). [https://doi.org/10.1016/0304-3975\(85\)90224-5](https://doi.org/10.1016/0304-3975(85)90224-5) 4

10. Hanson, A., Tu, A., Singla, V., Jayawardhana, M., Zwicker, M., Goldstein, T.: Pup 3d-gs: Principled uncertainty pruning for 3d gaussian splatting. In: Proceedings of the Computer Vision and Pattern Recognition Conference (CVPR). pp. 5949–5958 (June 2025), <https://pup3dgs.github.io/> 3
11. He, Y., Lin, J., Liu, Z., Wang, H., Li, L.J., Han, S.: Amc: Automl for model compression and acceleration on mobile devices. In: ECCV (2018), https://openaccess.thecvf.com/content_ECCV_2018/papers/Yihui_He_AMC_Automated_Model_ECCV_2018_paper.pdf 3
12. Jiang, Y., Zhang, L., Gao, J., Hu, W., Yao, Y.: Consistent4d: Consistent 360° dynamic object generation from monocular video. ArXiv **abs/2311.02848** (2023), <https://api.semanticscholar.org/CorpusID:265034292> 3
13. Kerbl, B., Kopanas, G., Leimkühler, T., Drettakis, G.: 3d gaussian splatting for real-time radiance field rendering. ACM Trans. Graph. **42**(4), 139–1 (2023) 2, 3
14. Kim, M., Kim, G., Choi, J., Roh, W., Han, B.: Physgaia: A physics-aware dataset of multi-body interactions for dynamic novel view synthesis. arXiv preprint arXiv:2506.02794 (2025) 3
15. Kirschstein, T., Qian, S., Giebenhain, S., Walter, T., Nießner, M.: Nersemble: Multi-view radiance field reconstruction of human heads. ACM Transactions on Graphics (TOG) **42**(4), 1–14 (2023) 3
16. Lang, I., Manor, A., Avidan, S.: Samplenet: Differentiable point cloud sampling. In: CVPR (2020), https://openaccess.thecvf.com/content_CVPR_2020/papers/Lang_SampleNet_Differentiable_Point_Cloud_Sampling_CVPR_2020_paper.pdf 3
17. Langford, J., Zhang, T.: The epoch-greedy algorithm for multi-armed bandits with side information. In: Advances in Neural Information Processing Systems 20 (NeurIPS 2007) (2007) 3
18. Lee, J., Lee, Y., Kim, J., Kosiorek, A., Choi, S., Teh, Y.W.: Set transformer: A framework for attention-based permutation-invariant neural networks. In: International Conference on Machine Learning (ICML) (2019) 3, 4
19. Lee, J., Won, C., Jung, H., Bae, I., Jeon, H.G.: Fully explicit dynamic gaussian splatting. Advances in Neural Information Processing Systems **37**, 5384–5409 (2024) 7
20. Li, H., Li, S., Gao, X., Batuer, A., Yu, L., Liao, Y.: Giftstream: 4d gaussian-based immersive video with feature stream. In: Proceedings of the Computer Vision and Pattern Recognition Conference. pp. 21761–21770 (2025) 3
21. Li, L., Chu, W., Langford, J., Schapire, R.E.: A contextual-bandit approach to personalized news article recommendation. In: Proceedings of the 19th International Conference on World Wide Web (WWW). pp. 661–670 (2010). <https://doi.org/10.1145/1772690.1772758> 3, 5
22. Li, L., Shen, Z., Wang, Z., Shen, L., Tan, P.: Streaming radiance fields for 3d video synthesis. In: Advances in Neural Information Processing Systems (NeurIPS) (2022), <https://arxiv.org/abs/2210.14831> 3, 6, 7, 8, 9, 14
23. Li, T., Slavcheva, M., Zollhoefer, M., Green, S., Lassner, C., Kim, C., Schmidt, T., Lovegrove, S., Goesele, M., Newcombe, R., et al.: Neural 3d video synthesis from multi-view video. In: Proceedings of the IEEE/CVF conference on computer vision and pattern recognition (CVPR). pp. 5521–5531 (2022) 3, 6
24. Li, T., Qiu, Y., Wu, Z., Lindström, C., Su, P., Nießner, M., Li, H.: Mtgs: Multi-traversal gaussian splatting. arXiv preprint arXiv:2503.12552 (2025) 3
25. Li, Z., Chen, Z., Li, Z., Xu, Y.: Spacetime gaussian feature splatting for real-time dynamic view synthesis. In: Proceedings of the IEEE/CVF Conference on Computer Vision and Pattern Recognition (CVPR). pp. 8508–8520 (June 2024) 3

26. Li, Z., Niklaus, S., Snavely, N., Wang, O.: Neural scene flow fields for space-time view synthesis of dynamic scenes. 2021 IEEE/CVF Conference on Computer Vision and Pattern Recognition (CVPR) pp. 6494–6504 (2020), <https://api.semanticscholar.org/CorpusID:227208781> 3
27. Loshchilov, I., Hutter, F.: Decoupled weight decay regularization. In: International Conference on Learning Representations (ICLR) (2019) 6
28. Lu, C.Y., Zhou, P., Xing, A., Pokhariya, C., Dey, A., Shah, I.N., Mavidipalli, R., Hu, D., Comport, A.I., Chen, K., et al.: Diva-360: The dynamic visual dataset for immersive neural fields. In: Proceedings of the IEEE/CVF Conference on Computer Vision and Pattern Recognition. pp. 22466–22476 (2024) 3
29. Mildenhall, B., Srinivasan, P.P., Tancik, M., Barron, J.T., Ramamoorthi, R., Ng, R.: Nerf: Representing scenes as neural radiance fields for view synthesis. *Communications of the ACM* **65**(1), 99–106 (2021) 2, 3
30. Nießner, M., Zollhöfer, M., Izadi, S., Stamminger, M.: Real-time 3d reconstruction at scale using voxel hashing. *ACM Transactions on Graphics* **32**(6), 169:1–169:11 (2013). <https://doi.org/10.1145/2508363.2508374> 4
31. Oh, S., Lee, Y., Jeon, H., Park, E.: Hybrid 3d-4d gaussian splatting for fast dynamic scene representation. arXiv preprint arXiv:2505.13215 (2025) 3, 7
32. Park, K., Sinha, U., Hedman, P., Barron, J.T., Bouaziz, S., Goldman, D.B., Martin-Brualla, R., Seitz, S.M.: Hypernerf. *ACM Transactions on Graphics (TOG)* **40**, 1–12 (2021), <https://api.semanticscholar.org/CorpusID:235624060> 3
33. Park, K., Sinha, U., Barron, J.T., Bouaziz, S., Goldman, D.B., Seitz, S.M., Martin-Brualla, R.: Nerfies: Deformable neural radiance fields. In: Proceedings of the IEEE/CVF international conference on computer vision. pp. 5865–5874 (2021) 3
34. Peng, S., Zhang, Y., Xu, Y., Wang, Q., Shuai, Q., Bao, H., Zhou, X.: Neural body: Implicit neural representations with structured latent codes for novel view synthesis of dynamic humans. In: CVPR (2021) 3
35. Pumarola, A., Corona, E., Pons-Moll, G., Moreno-Noguer, F.: D-NeRF: Neural Radiance Fields for Dynamic Scenes. In: Proceedings of the IEEE/CVF Conference on Computer Vision and Pattern Recognition (CVPR) (2020) 3
36. Qi, C.R., Yi, L., Su, H., Guibas, L.J.: Pointnet++: Deep hierarchical feature learning on point sets in a metric space. In: Advances in Neural Information Processing Systems (NeurIPS) (2017), <https://arxiv.org/abs/1706.02413> 2, 3, 4
37. Ren, K., Jiang, L., Lu, T., Yu, M., Xu, L., Ni, Z., Dai, B.: Octree-gs: Towards consistent real-time rendering with lod-structured 3d gaussians. *IEEE transactions on pattern analysis and machine intelligence* **PP** (2024), <https://api.semanticscholar.org/CorpusID:268691629> 3
38. Sabater, N., Boisson, G., Vandame, B., Kerbiriou, P., Babon, F., Hog, M., Gendrot, R., Langlois, T., Bureller, O., Schubert, A., Allié, V.: Dataset and pipeline for multi-view light-field video. In: 2017 IEEE Conference on Computer Vision and Pattern Recognition Workshops (CVPRW). pp. 1743–1753 (2017). <https://doi.org/10.1109/CVPRW.2017.221> 3
39. Shapovalov, R., Kleiman, Y., Rocco, I., Novotny, D., Vedaldi, A., Chen, C., Kokkinos, F., Graham, B., Neverova, N.: Replay: Multi-modal multi-view acted videos for casual holography. In: Proceedings of the IEEE/CVF International Conference on Computer Vision. pp. 20338–20348 (2023) 3
40. Sun, J., Jiao, H., Li, G., Zhang, Z., Zhao, L., Xing, W.: 3dgstream: On-the-fly training of 3d gaussians for efficient streaming of photo-realistic free-viewpoint videos. In: Proceedings of the IEEE/CVF Conference on Computer Vision and Pattern Recognition. pp. 20675–20685 (2024) 3, 6, 7, 8, 9, 14

41. Sutton, R.S., Barto, A.G.: Reinforcement Learning: An Introduction. MIT Press, 2 edn. (2018), <http://incompleteideas.net/book/the-book-2nd.html> 3, 5
42. Tu, A., Ying, H., Hanson, A., Lee, Y., Goldstein, T., Zwicker, M.: Speedy deformable 3d gaussian splatting: Fast rendering and compression of dynamic scenes. arXiv preprint arXiv:2506.07917 (2025), <https://speede3dgs.github.io/> 3
43. Vaswani, A., Shazeer, N., Parmar, N., Uszkoreit, J., Jones, L., Gomez, A.N., Kaiser, L., Polosukhin, I.: Attention is all you need. In: Advances in Neural Information Processing Systems (NeurIPS) (2017) 3, 4
44. Wang, L., Hu, Q., He, Q., Wang, Z., Yu, J., Tuytelaars, T., Xu, L., Wu, M.: Neural residual radiance fields for streamably free-viewpoint videos. In: Proceedings of the IEEE/CVF Conference on Computer Vision and Pattern Recognition (CVPR). pp. 76–87 (June 2023) 3
45. Wang, X., Yu, F., Dou, Z.Y., Darrell, T., Gonzalez, J.E.: Skipnet: Learning dynamic routing in convolutional networks. In: ECCV (2018), https://openaccess.thecvf.com/content_ECCV_2018/papers/Xin_Wang_SkipNet_Learning_Dynamic_ECCV_2018_paper.pdf 3
46. Wang, Y., Yang, P., Xu, Z., Sun, J., Zhang, Z., Chen, Y., Bao, H., Peng, S., Zhou, X.: Freetimegs: Free gaussian primitives at anytime anywhere for dynamic scene reconstruction. In: CVPR (2025), <https://zju3dv.github.io/freetimegs> 3
47. Wang, Z., Bovik, A.C., Sheikh, H.R., Simoncelli, E.P.: Image quality assessment: From error visibility to structural similarity. IEEE Transactions on Image Processing **13**(4), 600–612 (2004). <https://doi.org/10.1109/TIP.2003.819861>, <https://www.ece.utexas.edu/~bevans/courses/ee381k/lectures/ssim.pdf> 6
48. Williams, R.J.: Simple statistical gradient-following algorithms for connectionist reinforcement learning. Machine Learning **8**(3–4), 229–256 (1992) 3, 5
49. Wu, G., Yi, T., Fang, J., Xie, L., Zhang, X., Wei, W., Liu, W., Tian, Q., Wang, X.: 4d gaussian splatting for real-time dynamic scene rendering. In: Proceedings of the IEEE/CVF Conference on Computer Vision and Pattern Recognition (CVPR). pp. 20310–20320 (June 2024) 3
50. Wu, Z., Nagarajan, T., Kumar, A., Rennie, S., Davis, L.S., Grauman, K., Feris, R.: Blockdrop: Dynamic inference paths in residual networks. In: CVPR (2018), https://openaccess.thecvf.com/content_cvpr_2018/papers/Wu_BlockDrop_Dynamic_Inference_CVPR_2018_paper.pdf 3
51. Yan, J., Peng, R., Wang, Z., Tang, L., Yang, J., Liang, J., Wu, J., Wang, R.: Instant gaussian stream: Fast and generalizable streaming of dynamic scene reconstruction via gaussian splatting. In: Proceedings of the Computer Vision and Pattern Recognition Conference. pp. 16520–16531 (2025) 3, 4, 7, 8, 9, 14
52. Yang, Z., Gao, X., Zhou, W., Jiao, S., Zhang, Y., Jin, X.: Deformable 3d gaussians for high-fidelity monocular dynamic scene reconstruction. 2024 IEEE/CVF Conference on Computer Vision and Pattern Recognition (CVPR) pp. 20331–20341 (2023), <https://api.semanticscholar.org/CorpusID:262466218> 3
53. Yao, W., Xie, S., Li, L., Zhang, W., Lai, Z., Dai, S., Zhang, K., Wang, Z.: Sdgs: Structured deformable 3d gaussians for efficient dynamic scene reconstruction. arXiv preprint arXiv:2507.07465 (2025) 7
54. Yin, M., Cao, Y., Peng, S., Han, K.: Splat4d: Diffusion-enhanced 4d gaussian splatting for temporally and spatially consistent content creation. In: Proceedings of the Special Interest Group on Computer Graphics and Interactive Techniques Conference Conference Papers. pp. 1–10 (2025) 3
55. Yuan, Y., et al.: Efficient differentiable hardware rasterization for 3d gaussian splatting. arXiv preprint arXiv:2505.18764 (2025) 3

56. Zhang, R., Isola, P., Efros, A.A., Shechtman, E., Wang, O.: The unreasonable effectiveness of deep features as a perceptual metric. In: Proceedings of the IEEE/CVF Conference on Computer Vision and Pattern Recognition (CVPR) (2018). <https://doi.org/10.48550/arXiv.1801.03924>, <https://arxiv.org/abs/1801.03924> 6
57. Zheng, X., Liao, L., Li, X., Jiao, J., Wang, R., Gao, F., Wang, S., Wang, R.: Pku-dymvhumans: A multi-view video benchmark for high-fidelity dynamic human modeling. In: Proceedings of the IEEE/CVF Conference on Computer Vision and Pattern Recognition. pp. 22530–22540 (2024) 3